Gels of DNA Nanostars Never Crystallize

Lorenzo Rovigatti,[†,*] Frank Smallenburg,[†] Flavio Romano,[‡] and Francesco Sciortino[†]

[†]Dipartimento di Fisica, Sapienza Università di Roma, Piazzale A. Moro 2, 00185 Roma, Italy and [‡]Physical & Theoretical Chemistry Laboratory, Department of Chemistry, University of Oxford, South Parks Road, Oxford OX1 3QZ, United Kingdom

ABSTRACT Using state-of-the-art numerical techniques, we show that, upon lowering the temperature, tetravalent DNA nanostars form a *thermodynamically stable*, fully bonded equilibrium gel. In contrast to atomic and molecular network formers, in which the disordered liquid is always metastable with respect to some crystalline phase, we find that the DNA nanostar gel has a lower free energy than the diamond crystal structure in a wide range of concentrations. This unconventional behavior, here verified for the first time in a realistic model, arises from the large arm flexibility of the DNA nanostars, a property that can be tuned by design. Our results confirm the thermodynamic stability of the recently experimentally realized DNA hydrogels.

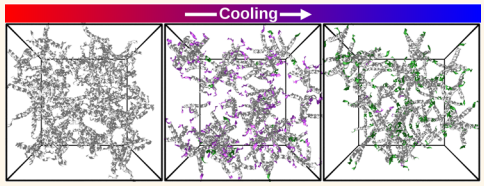

KEYWORDS: physical gels · DNA hydrogels · DNA nanostars · DNA self-assembly

The main biological role of DNA is to store and readily provide genetic information. This information is encoded in the linear arrangement of the four different bases (adenine, thymine, cytosine, and guanine) along the DNA polymer that effectively provides a four-letter alphabet, with the direction being encoded through the chirality of the molecule. The Watson–Crick pairing causes DNA nucleotides to bind selectively in pairs, adenine with thymine and cytosine with guanine.[1] This binding specificity is essential in nature to accurately replicate genetic code but has the potential to be artificially exploited to design DNA constructs that assemble in a programmable way.[2] Advances in materials science and nanotechnology show that the DNA pairing mechanism offers numerous possibilities for realizing nano- and mesoscopic supramolecular constructs entirely made up of DNA.[3,4] Molecular machines,[5,6] DNA origami,[7,8] DNA logic gates,[9] and DNA polyhedra[10] are relevant examples of what can be done by carefully designing DNA strand sequences and mixing them in solution in the right external conditions. Here we focus on DNA nanostars,[11,12] that is, DNA constructs with four arms ending with sticky ends, whose collective phase behavior has been recently experimentally and numerically investigated.[13,14] These limited valence supramolecules behave in solution similarly to molecules, exhibiting at low temperature a gas (DNA-poor) and a liquid (DNA-rich) phase, separated by a first-order transition line ending in a second-order critical point.[13] Interestingly, the liquid phase is formed by a percolating network of four functional nodes, giving rise to a physical (reversible) gel.[15] In systems without a limited valence, where particles do not have a fixed maximum number of bonded neighbors, the interplay between energy and entropy always starts favoring lower-energy states as the temperature T is decreased. At low temperature, the system reaches its ground state, which is typically an ordered, crystalline structure. In the framework of limited valence particles, on the other hand, the maximum number of bonds (and hence the ground state energy) is fixed by the particle valence. In recent years, it has been shown that in limited valence systems it is possible to form fully bonded disordered states at finite temperature in a wide range of densities.[16,17] These fully bonded states have the same potential energy as the fully bonded crystal and can thus compete for stability with the crystal phase even at very low T. Once the system is in its fully bonded disordered state, a further decrease of the temperature has only a small effect on its dynamics. The number of bonds and the network topology (*i.e.*, the statistics of the network rings) have reached their

* Address correspondence to lorenzo.rovigatti@uniroma1.it.

Received for review January 2, 2014 and accepted March 19, 2014.

Published online March 19, 2014
10.1021/nn501138w

ground state values and retain them if the temperature is further lowered. This property also holds for the ordered phase, so that the relative stability of the ordered and disordered phases, if accessed at a temperature for which both phases are fully bonded, is also retained for lower T. In the following, we will refer to the temperature at which the system reaches its fully bonded state as the *low-temperature limit*. As we will show, for the system under study and for the concentrations considered, the fully bonded state is reached around $T \approx 30$ °C and is thus experimentally accessible. Building on this, it has been recently speculated that limited valence and flexible bonds are the two key ingredients for the formation of what can be considered a previously unexplored state of matter: the thermodynamically stable fully bonded disordered network state.[18] This state forms through the progressive establishment of all possible bonds, without the intervention of either a more stable crystal phase or a phase separation.[18,19] The possibility of averting the normal ordering typical of atomic and molecular fluids (with the exception of helium) and giving rise to disordered states more stable than ordered ones thus relies on the limited valence of the particles since both the crystal and the network fluid can be in a fully bonded configuration at finite T, ensuring that their relative thermodynamic stability is purely controlled by entropy. The interplay between vibrational entropy, which is larger in the crystal, and configurational entropy, which is larger in the network,[18] can be tuned by controlling the bond flexibility. Theoretical predictions based on a primitive patchy model suggest that with increasing flexibility the configurational part of the entropy outbalances the vibrational part; this stabilizes a disordered, fully bonded network in a wide range of concentrations.[18]

In this work, we show that the experimentally investigated tetravalent DNA nanostars[13] are indeed sufficiently flexible to provide the first soft-matter example of a liquid more stable than a crystal. We provide strong evidence by simulating a bulk system of DNA tetramers using a realistic DNA model and calculating, despite the complexity of the particles and of their self-assembly, the free energies of the liquid and of the crystal phases. Our free-energy calculations reveal that the fluid is substantially more stable than the crystal in a very wide range of concentrations and in an experimentally accessible range of temperatures. We thus provide a solid background for experimental realizations of DNA hydrogels, which are shown here to be thermodynamically stable. This is different from the case of more common colloidal gels (*e.g.*, gels in which colloidal particles interact *via* polymer-induced depletion interactions[20]) or of other soft-matter arrested states[21,22] in which the system is kinetically trapped in an out-of-equilibrium condition. In this last class of systems, an extremely long time, possibly much longer than any reasonable observation time, is required to observe crystallization. By contrast, in DNA hydrogels, crystallization is guaranteed to never take place.

Strand sequences
CGCGGTCGCGGCTTCCGACTCGCACGTCGATCG
CGGTGAGGTGCGTTGCCGCCCGAGGCTCGATCG
GCCTCGGGCGGCTTGCCGCGACCGCGTCGATCG
CGTGCGAGTCGGTTCGCACCTCACCGTCGATCG

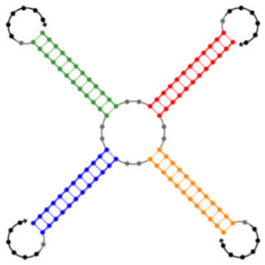

Figure 1. Top: Strand sequences investigated in this work, designed to self-assemble into tetravalent all-DNA nanostars. Colored nucleotides form the double-stranded parts of the arms, with complementary sequences sharing the same color. Spacers are colored in gray and sticky ends in black. Bottom: Schematic representation of a DNA nanostar. The color coding is the same as in the table.

RESULTS

In recent years, several coarse-grained models of DNA at the nucleotide level have been proposed.[23−29] We simulate DNA constructs with oxDNA, a coarse-grained model parametrized to reproduce the structure and the thermodynamics of single- (ssDNA) and double-stranded (dsDNA) molecules of DNA.[27,30] The model has been used to investigate a large variety of systems, encompassing DNA nanotechnology applications and DNA liquid crystals.[30−33]

We investigate DNA nanostars made up of four strands, each containing 33 nucleotides. Strand sequences are reported in Figure 1. The four sequences can be divided into three regions separated by one or two nucleotides that, acting as spacers, increase the flexibility of the tetramer. The first two regions are 12 bases long and are designed in such a way that they bind in complementary pairs to form the double-stranded parts of the tetramer arms. Below 65 °C, the system is composed of (weakly interacting) self-assembled tetramers. The third region, composed of six nucleotides, is identical in all four sequences and self-complementary. This final sequence acts as a sticky end, allowing for intertetramer bonds. The difference in length between the double-stranded arms and the sticky ends provides a separation between the temperature at which the nanostars assemble and the temperature at which the nanostars start to form a network. If collective effects are ignored, the two temperatures are about 35 K apart. The double-stranded sections of the arms are quite short and thus very stiff, while the arm flexibility is provided by the unpaired TT bases (gray in Figure 1) that are present at

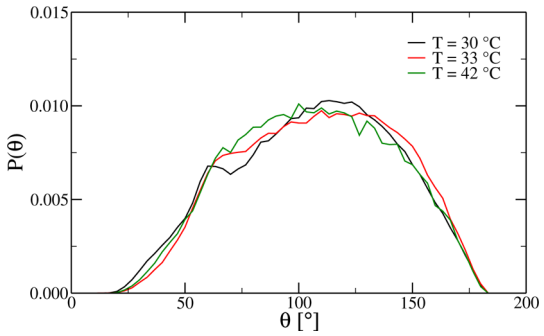

Figure 2. Distribution of the angle θ between the centers of mass of all bonded triplets for different temperatures.

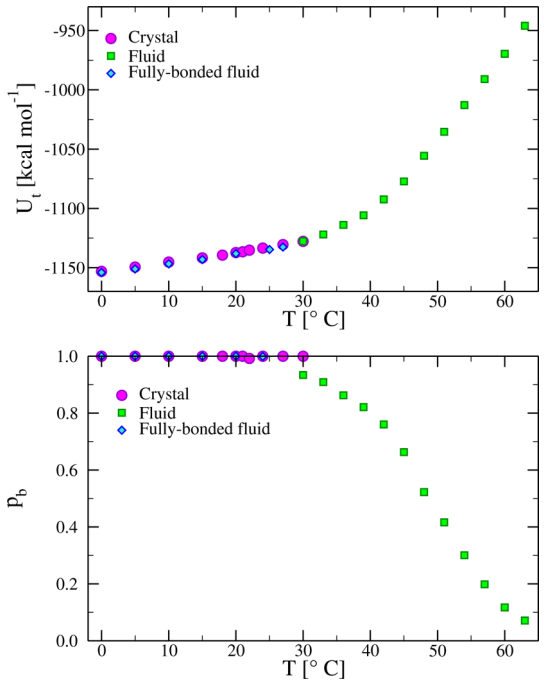

Figure 3. (a) Internal energy per mole of nanostars U_t for the crystal (magenta circles) and for the fluid (green squares) as a function of temperature T at c = 1.5 mM. (b) Fraction of formed bonds p_b as a function of T at the same concentration.

the center of the structure and before the reactive ends. Since it is our hypothesis that this arm flexibility stabilizes the gel state at low T, we assess it by computing the distributions $P(\theta)$ of the angle θ formed by all bonded nanostar triplets. Results for $P(\theta)$ at different T in the fluid phase are shown in Figure 2. The distribution is centered around the tetrahedral angle 109.5°. The width of the distributions is very large, demonstrating that DNA nanostars are highly flexible, independently of T. The distributions are even wider than those studied in the patchy primitive model which displays a thermodynamically stable gel.[18,34] Hence, based on theoretical predictions,[18] DNA nanostars should form a thermodynamically stable fully bonded state at low T and provide the first realistic example of this unconventional state of matter.

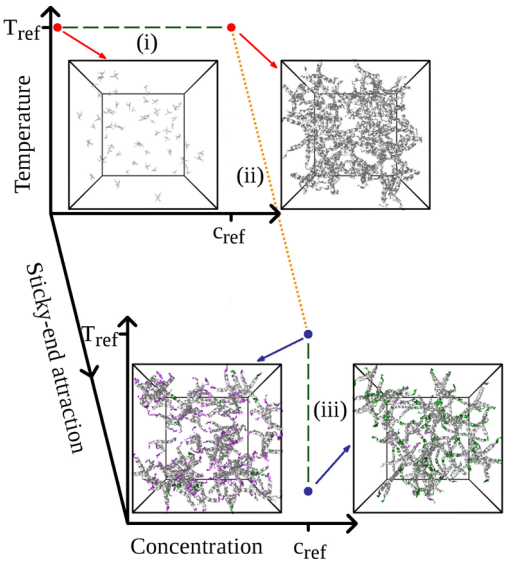

Figure 4. Cartoon of the protocol employed to compute the free energy of the fluid phase. Green dashed lines signal thermodynamic integration, whereas the orange dotted line represents a Hamiltonian integration path, connecting a system of tetramers with switched-off sticky ends to the fully interacting fluid. The integration paths are numbered according to the steps described in the Model and Methods section. The snapshots show typical configurations at the marked state points. Here, DNA strands are colored according to the following scheme: DNA sequences interacting only through excluded volume are in gray, unbound sticky ends are in violet, and bound ones are in green.

Figure 3 shows the total internal energy, U_t, and the fraction of formed bonds, p_b, as a function of T for both the fluid and crystal phase. In the fluid phase, as T is lowered, tetramers start to form larger and larger clusters, until they eventually form a network spanning the entire system. We are able to sample equilibrium in the fluid down to T = 30 °C, a temperature at which all tetramers are part of the same percolating cluster and $p_b \approx 0.94$. Equilibration at lower T is made prohibitive by the slow relaxation time of the network, which requires breaking and re-forming of intertetramer bonds. Since in the region $p_b > 0.94$ (corresponding approximately to $T < 30$ °C) it is impossible to provide equilibrium data in the fluid state, we exploit the possibility of simulating lower T by starting the simulation in a fully bonded, disordered configuration, as explained in the Model and Methods section, and extrapolating the data in the short missing T interval. Since the employed bonding pattern might not be optimal for the DNA nanostars, the results will underestimate the stability of the fluid. The fluid U_t exhibits a clear change in steepness at a T very close to the melting temperature of the sticky ends, $T \approx 40$ °C. Below this T, the majority of the intertetramer bonds are formed, and the energy change is mostly due to intratetramer vibrational terms. We note that, on the scale of the plot, the energy of the crystal and of the fully bonded fluid appear to be the same, whereas they differ by about 1.8 kcal/mol at T = 24 °C, with this

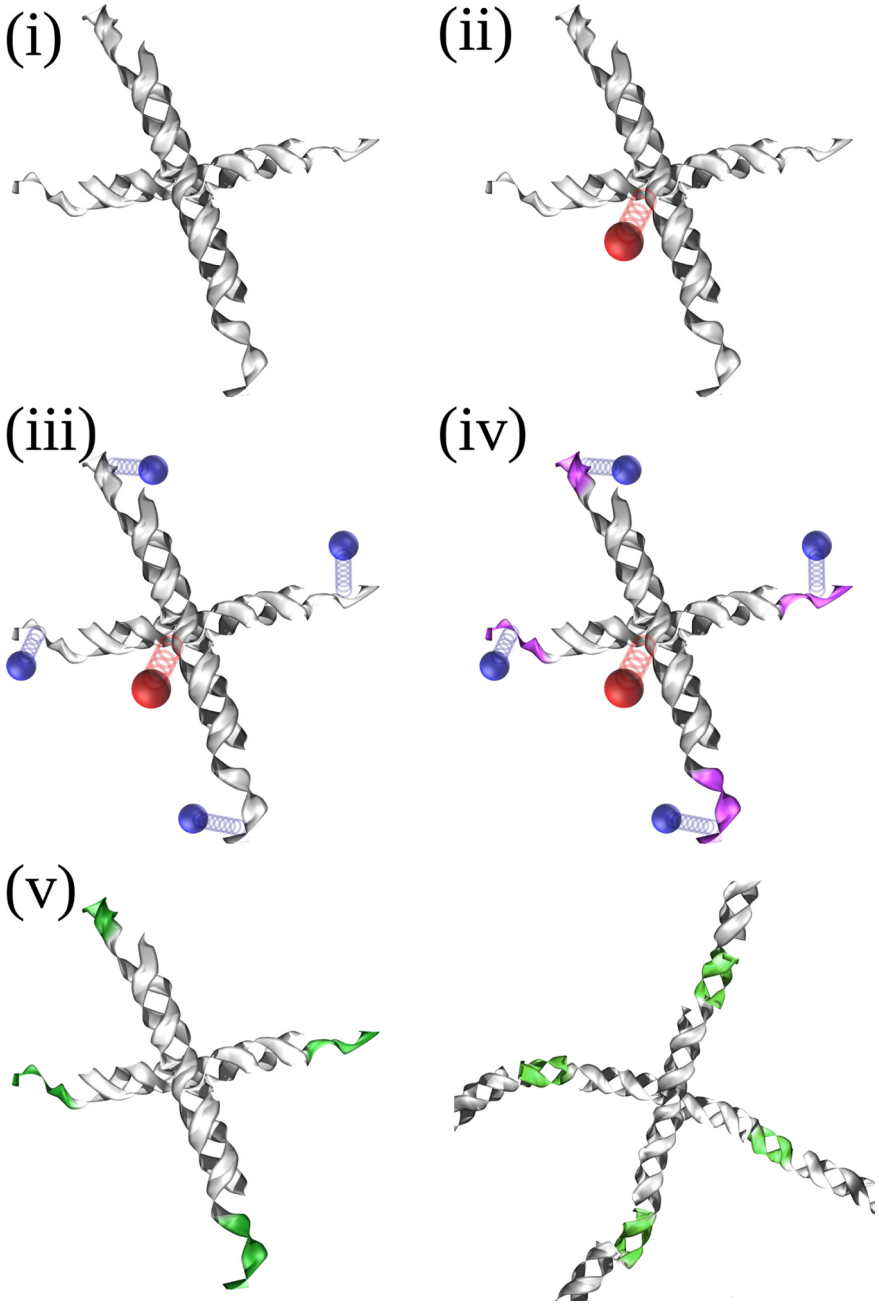

Figure 5. Cartoon of the protocol employed to compute the free energy of the crystal. The steps are numbered according to the protocol described in the Model and Methods section. DNA strands are color-coded as in Figure 4. The last panel shows a tetramer bound to the arms of four other tetramers in the crystal structure.

difference not changing much as the system is cooled down. Quite surprisingly, the fully bonded fluid is the one having the lowest potential energy in the explored T range. Since the number of base pairs is the same in the two systems, we attribute this difference to a slightly higher degree of stress present in the crystal.

To make sure that finite size effects were not present in our simulations of the crystal, we have repeated the potential energy calculations at $T = 20$ °C for systems with 216 tetramers. The average potential energies obtained were indistinguishable.

In order to assess the thermodynamic stability of the ordered and disordered phases, we calculate the Helmholtz free energy of the fluid and of the crystal. Tetrahedrally coordinated particles are compatible with a large number of crystalline arrangements; indeed, the quest for low-pressure, tetrahedrally coordinated crystal phases is a science of its own,[35,36] but in all cases, the most stable phase is always a diamond phase, either cubic or hexagonal.[37−40] For systems with a short-range attraction such as the one under study, the two morphologies are almost indistinguishable because they have been shown to have the same

energy, entropy, and density in a wide range of pressure and temperature.[38,41] Since it would be impractical to consider all these phases, we focus only on the diamond cubic (DC) as the candidate structure, assuming that the hexagonal diamond will have the same free energy and all other tetrahedral arrangements will have a comparable or higher free energy.

Although our procedure to estimate the free energy requires several steps, these are all variations of thermodynamic or Hamiltonian integration.[42,43] These techniques provide free-energy differences between two state points by integrating derivatives of the free energy along a pathway that connects the two state points. The procedures required to compute the free energy of the fluid and of the crystal are sketched in Figures 4 and 5, respectively, and thoroughly described in the Model and Methods section and in the Supporting Information (SI).

Figure 6 shows the main result of this work: the free energies of the crystal, of the fluid, and the difference thereof, calculated at $T = 24$ °C (where the fluid is fully bonded) as a function of c. The concentration range spans the entire region where the fully bonded network exists. The two free energies are well separated, and no common tangent construction is possible, leading to the conclusion that there is no coexistence between the fluid and the crystal in the wide range of concentrations considered here. We also compute the chemical potential as the Gibbs free energy per particle, $\mu = (F + PV)/N$, where P is the osmotic pressure, V is the volume of the system, and N is the number of tetramers. Since coexisting phases share the same values of T, P, and μ, we check that there is no phase separation by plotting $\mu(P)$ for the fluid and for the crystal. The resulting lines, shown in Figure 6b, are well separated and almost parallel, confirming that no phase separation occurs in the explored concentration range. Contrary to what happens in the great majority of systems, the DNA nanostar fully bonded liquid is thermodynamically stable in the whole concentration range investigated here. The difference in free energy $\Delta f(c,T)$, presented in Figure 6c, decreases as c increases until it reaches a plateau. The difference between internal energies can only partially account for this large free-energy difference since $U_t^{cryst} - U_t^{fluid}$ never exceeds 2 kcal/mol and does not grow upon lowering T. The remaining part of $\Delta f(c,T)$, more than 0.6 kcal/mol, stems from the difference between vibrational entropy and configurational entropy. The former, connected to the volume of the phase space explorable at a fixed bonding pattern, is higher in the crystal due to the better packing achieved by ordered structures with respect to disordered ones. The latter, on the other hand, is linked to the number of unique realizations of bonding patterns that result in the same macroscopic state. The crystal under study has only one possible realization. By contrast, there is more than one way of

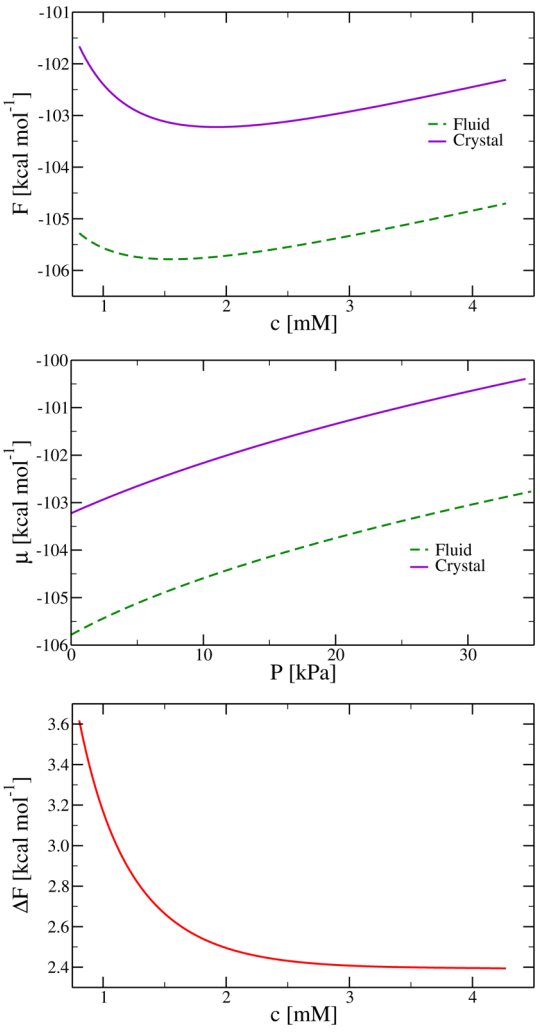

Figure 6. (a) Free energy F of the crystal (solid violet line) and of the fluid (dashed green line) as a function of tetramer concentration. (b) Chemical potential μ as a function of osmotic pressure P for the crystal (solid violet line) and the fluid (dashed green line). (c) Difference $\Delta F = F_{cryst} - F_{fluid}$ between the free energy of the crystal and the free energy of the fluid.

realizing a disordered fully bonded network, and hence the configurational entropy is always higher in fluids. Interestingly, the entropy difference we find is on the same order as the corresponding quantity evaluated in primitive models with similar flexibility.[18] The 0.6 kcal/mol difference ($\approx 1 k_B T$ per nanostar, where k_B is the Boltzmann constant) exceeds the statistical error associated with the numerical procedure and possible contributions due to finite size effects, both of which are on the order of 0.05 kcal/mol.

CONCLUSIONS

Atomic and molecular systems unavoidably have some ordered crystal as the equilibrium phase in the low-temperature limit. The simple explanation for this ubiquitous phenomenon is that the crystalline arrangement maximizes the number of contacts, thus optimizing the potential energy of the system which dominates the free energy at low T. However, there are

two more factors that usually promote the stability of crystals: both packing and vibrational entropy are maximized, further favoring ordered *versus* disordered states. The configurational entropy is the only thermodynamic drive which is still higher in the liquid.

Low-valence systems can reach the potential energy ground state in the disordered liquid phase at finite temperatures, removing the dominant energetic factor that stabilizes the crystal. Also, the relevant crystals at low pressure have a density comparable to that of the liquid, so that crystals have no substantial packing advantage either. The competition is thus solely on entropic grounds, and it is possible that the configurational entropy of the disordered fully bonded states (linked to the number of ways the latter can be realized) can outbalance the higher vibrational entropy that particles experience in the crystal. The bond flexibility is the key ingredient in making this possible, as recently shown for a primitive model with limited valence.[18]

The recently synthesized tetravalent DNA nanostars are a good candidate for providing the first soft-matter example of a liquid more stable than a crystal. They indeed possess both key ingredients: limited valence and large arm flexibility, both of which can be finely tuned by design. Studying a realistic and quantitative model for these nanoparticles at 0.5 M Na^+ concentration, we have shown that the star arm flexibility is in the regime for which the thermodynamic stability of the low T fluid is predicted.[18] More importantly, by accurately evaluating the free energy of both crystal and fluid states, we have shown that the chemical potential of the liquid state is lower than the one of the crystal state in a wide range of concentrations. Even though we have shown that the chemical potential of the fluid is lower than that of the crystal at $T = 24$ °C, the fact that the comparison involves two phases which are both fully bonded implies that a further decrease of the temperature does not alter their relative stability. DNA gels are more stable than the corresponding crystal phases down to the temperature where the freezing of the solvent prevents further observations. Our calculations show that crystallization can be avoided by design and provides a theoretical background for the realization of fully bonded equilibrium gels. Differently from colloidal gels based on depletion interactions, or from arrested states of matter driven by a glass transition, in DNA gels, the absence of crystallization, observed on experimental time scales, is not a nonequilibrium effect but arises from the thermodynamic stability of the fluid phase: DNA nanostar gels will never crystallize.

MODEL AND METHODS

Model. The basic unit of the model is a nucleotide, modeled as a rigid body interacting with its neighbors through a complex set of highly anisotropic interactions that reproduce the structure and mechanical properties of stiff double helices and flexible single-stranded DNA. The model has been parametrized to reproduce the melting temperature of DNA duplexes as a function of length at a fixed monovalent salt concentration of 0.5 M. OxDNA has been tested on a number of systems, consistently showing very good agreement with experiments.[44−47]

The relevant features of the oxDNA model that we exploit are the quantitative thermodynamic predictions for the melting of duplexes and the ability to reproduce the different flexibility of double- and single-stranded DNA. Both quantities are indeed very well captured by oxDNA. We should note that oxDNA does not reproduce the major and minor groove of duplex DNA, a feature that might yield unrealistic results for the structure of tight four-way junctions, but the junctions in our systems are designed to avoid this problem.

Simulations. We perform Brownian dynamics simulations in the NVT ensemble to investigate bulk systems composed of 64 tetramers, for a total of 8448 nucleotides. Such a large number of nucleotides is highly demanding from a numerical point of view, and therefore, we carry out all computations with the GPU-enabled version of oxDNA, which is 30−50 times faster than its CPU counterpart on such large systems. The simulations start from a configuration of isolated tetramers and proceed in time until the energy (or equivalently the number of interstar bonds) equilibrates. We also perform studies of a diamond crystal, equilibrating an initial configuration in which the centers of the stars are located on a perfect cubic diamond lattice and the arms are properly oriented to facilitate the formation of sticky end bonds with the four nearest neighbors. Finally, to provide a reference energy for the fully bonded liquid, we perform low T simulations starting from a fully bonded disordered pattern in which the location of the star centers and the orientation of the star arms are extracted from a fully bonded configuration of tetravalent Kern−Frenkel[48] patchy particles with a patch width selected to match the DNA nanostars. All simulations have been performed with the oxDNA molecular simulation package, which is freely available online.[49] In total, the simulations ran for more than 4 months on six GPUs.

Free-Energy Calculation. In the following, we only sketch the steps taken to compute the free energy, while all the details are provided in the SI. The free energy of the fluid is calculated with respect to an ideal gas of tetramers with switched-off sticky ends (where the base-pairing interaction has been disabled only for the sticky end nucleotides; see SI) at $T_{ref} = 60$ °C and at a sufficiently low concentration c to consider them noninteracting. The thermodynamic integration is performed according to the following steps. (i) We integrate the equation of state (at T_{ref}) of a system of tetramers in which the sticky end interactions are switched off, increasing the concentration from the ideal gas regime to $c = c_{ref}$. (ii) We gradually turn on the interactions between the tetramers at T_{ref}, evaluating the free-energy difference between the interacting and noninteracting fluid by a standard Hamiltonian integration.[43] (iii) We lower T, integrating the potential energy to evaluate the free-energy difference between T_{ref} and T. (iv) Finally, to estimate the fluid free energy $f_{fluid}(c,T)$ as a function of the tetramer concentration, we integrate along the numerically evaluated equation of state at fixed T. A sketch of the process is presented in Figure 4.

In order to compute the free energy of the diamond crystal, we develop an extension of the Einstein crystal technique,[50] adapted for DNA nanostars. Also in this case, to evaluate the free-energy difference with respect to an ideal gas of noninteracting tetramers, we proceed in a series of thermodynamic integration steps. (i) We integrate the temperature dependence of the potential energy from T_{ref} to T for noninteracting tetramers at effectively zero concentration. (ii) We attach the noninteracting tetramers to an ideal diamond lattice *via* harmonic springs acting on one of the central nucleotides in each tetramer, generating the Einstein cubic DC.[50] The free-energy

change associated with this step is the free-energy difference between an ideal Einstein crystal and the ideal gas and can be calculated analytically. (iii) In the next step, we gradually turn on, for each arm, harmonic springs on one of the sticky end nucleotides of the (still noninteracting) tetramers, restricting their orientations. The free-energy change is obtained by integrating the potential energy associated with the harmonic wells. (iv) We turn on the interactions between the tetramers, as in the fluid step (ii), while maintaining the springs on the tetramer centers and arms. (v) To complete the thermodynamic path, we progressively turn off all springs attached to the tetramers, again calculating the free-energy difference by integrating the harmonic potential energy. As in the case of the fluid, integration along the crystal equation of state provides the free energy of the crystal as a function of c and T, namely, $f_{cryst}(c,T)$. Figure 5 presents a cartoon of the procedure.

Conflict of Interest: The authors declare no competing financial interest.

Acknowledgment. We acknowledge support from ERC-226207-PATCHYCOLLOIDS, MIUR-PRIN, and NVIDIA.

Supporting Information Available: (i) A description of the units of measurement used in the oxDNA model, (ii) a thorough description of the procedure employed to compute the free energy of the fluid and of the crystal, and (iii) plots of the simulation output used as input for the free-energy calculations. This material is available free of charge *via* the Internet at http://pubs.acs.org.

REFERENCES AND NOTES

1. Watson, J. D.; Crick, F. H. Molecular Structure of Nucleic Acids. *Nature* **1953**, *171*, 737–738.
2. Seeman, N. DNA in a Material World. *Nature* **2003**, *421*, 427–431.
3. Seeman, N. C. DNA Nanotechnology: Novel DNA Constructions. *Annu. Rev. Biophys. Biomol. Struct.* **1998**, *27*, 225–248.
4. Lee, J. B.; Peng, S.; Yang, D.; Roh, Y. H.; Funabashi, H.; Park, N.; Rice, E. J.; Chen, L.; Long, R.; Wu, M.; *et al.* A Mechanical Metamaterial Made from a DNA Hydrogel. *Nat. Nanotechnol.* **2012**, *7*, 816–820.
5. Ouldridge, T. E.; Hoare, R. L.; Louis, A. A.; Doye, J. P. K.; Bath, J.; Turberfield, A. J. Optimizing DNA Nanotechnology through Coarse-Grained Modeling: A Two-Footed DNA Walker. *ACS Nano* **2013**, *7*, 2479–2490.
6. Wollman, A. J.; Sanchez-Cano, C.; Carstairs, H. M.; Cross, R. A.; Turberfield, A. J. Transport and Self-Organization Across Different Length Scales Powered by Motor Proteins and Programmed by DNA. *Nat. Nanotechnol.* **2013**, *9*, 44–47.
7. Rothemund, P. Folding DNA To Create Nanoscale Shapes and Patterns. *Nature* **2006**, *440*, 297–302.
8. Yang, Y.; Han, D.; Nangreave, J.; Liu, Y.; Yan, H. DNA Origami with Double-Stranded DNA as a Unified Scaffold. *ACS Nano* **2012**, *6*, 8209–8215.
9. Soloveichik, D.; Seelig, G.; Winfree, E. DNA as a Universal Substrate for Chemical Kinetics. *Proc. Natl. Acad. Sci. U.S.A.* **2010**, *107*, 5393–5398.
10. He, Y.; Ye, T.; Su, M.; Zhang, C.; Ribbe, A. E.; Jiang, W.; Mao, C. Hierarchical Self-Assembly of DNA into Symmetric Supramolecular Polyhedra. *Nature* **2008**, *452*, 198–201.
11. Seeman, N. C. Nucleic Acid Junctions and Lattices. *J. Theor. Biol.* **1982**, *99*, 237–247.
12. Roh, Y. H.; Ruiz, R. C. H.; Peng, S.; Lee, J. B.; Luo, D. Engineering DNA-Based Functional Materials. *Chem. Soc. Rev.* **2011**, *40*, 5730–5744.
13. Biffi, S.; Cerbino, R.; Bomboi, F.; Paraboschi, E. M.; Asselta, R.; Sciortino, F.; Bellini, T. Phase Behavior and Critical Activated Dynamics of Limited-Valence DNA Nanostars. *Proc. Natl. Acad. Sci. U.S.A.* **2013**, *110*, 15633–15637.
14. Rovigatti, L.; Bomboi, F.; Sciortino, F. Accurate Phase Diagram of Tetravalent DNA Nanostars. *arXiv:1401.2837v1* **2014**.
15. Bianchi, E.; Largo, J.; Tartaglia, P.; Zaccarelli, E.; Sciortino, F. Phase Diagram of Patchy Colloids: Towards Empty Liquids. *Phys. Rev. Lett.* **2006**, *97*, 168301–168304.
16. Russo, J.; Tartaglia, P.; Sciortino, F. Reversible Gels of Patchy Particles: Role of the Valence. *J. Chem. Phys.* **2009**, *131*, 014504.
17. Rovigatti, L.; Kob, W.; Sciortino, F. The Vibrational Density of States of a Disordered Gel Model. *J. Chem. Phys.* **2011**, *135*, 104502.
18. Smallenburg, F.; Sciortino, F. Liquids More Stable than Crystals in Particles with Limited Valence and Flexible Bonds. *Nat. Phys.* **2013**, *9*, 554–558.
19. Martinez-Veracoechea, F. J.; Mladek, B. M.; Tkachenko, A. V.; Frenkel, D. Design Rule for Colloidal Crystals of DNA-Functionalized Particles. *Phys. Rev. Lett.* **2011**, *107*, 045902.
20. Lu, P. J.; Zaccarelli, E.; Ciulla, F.; Schofield, A. B.; Sciortino, F.; Weitz, D. A. Gelation of Particles with Short-Range Attraction. *Nature* **2008**, *453*, 499–503.
21. Foffi, G.; Sciortino, F.; Tartaglia, P.; Zaccarelli, E.; Verso, F. L.; Reatto, L.; Dawson, K. A.; Likos, C. N. Structural Arrest in Dense Star-Polymer Solutions. *Phys. Rev. Lett.* **2003**, *90*, 238301.
22. Dawson, K. A. The Glass Paradigm for Colloidal Glasses, Gels, and Other Arrested States Driven by Attractive Interactions. *Curr. Opin. Colloid Interface Sci.* **2002**, *7*, 218–227.
23. Starr, F. W.; Sciortino, F. Model for Assembly and Gelation of Four-Armed DNA Dendrimers. *J. Phys.: Condens. Matter* **2006**, *18*, L347–L353.
24. Knotts, T. A.; Rathore, N.; Schwartz, D. C.; de Pablo, J. J. A Coarse Grain Model for DNA. *J. Chem. Phys.* **2007**, *126*, 4901.
25. Knorowski, C.; Burleigh, S.; Travesset, A. Dynamics and Statics of DNA-Programmable Nanoparticle Self-Assembly and Crystallization. *Phys. Rev. Lett.* **2011**, *106*, 215501.
26. Li, T. I.; Sknepnek, R.; Macfarlane, R. J.; Mirkin, C. A.; Olvera de la Cruz, M. Modeling the Crystallization of Spherical Nucleic Acid Nanoparticle Conjugates with Molecular Dynamics Simulations. *Nano Lett.* **2012**, *12*, 2509–2514.
27. Ouldridge, T. E. Coarse-Grained Modelling of DNA and DNA Self-Assembly. Ph.D. Thesis, University of Oxford, 2011.
28. Hsu, C. W.; Fyta, M.; Lakatos, G.; Melchionna, S.; Kaxiras, E. *Ab Initio* Determination of Coarse-Grained Interactions in Double-Stranded DNA. *J. Chem. Phys.* **2012**, *137*, 105102.
29. Hinckley, D. M.; Freeman, G. S.; Whitmer, J. K.; de Pablo, J. J. An Experimentally-Informed Coarse-Grained 3-Site-per-Nucleotide Model of DNA: Structure, Thermodynamics, and Dynamics of Hybridization. *J. Chem. Phys.* **2013**, *139*, 144903.
30. Ouldridge, T. E.; Louis, A. A.; Doye, J. P. K. Structural, Mechanical, and Thermodynamic Properties of a Coarse-Grained DNA model. *J. Chem. Phys.* **2011**, *134*, 085101.
31. Ouldridge, T. E.; Louis, A. A.; Doye, J. P. K. DNA Nanotweezers Studied with a Coarse-Grained Model of DNA. *Phys. Rev. Lett.* **2010**, *104*, 178101.
32. Šulc, P.; Romano, F.; Ouldridge, T. E.; Rovigatti, L.; Doye, J. P. K.; Louis, A. A. Sequence-Dependent Thermodynamics of a Coarse-Grained DNA Model. *J. Chem. Phys.* **2012**, *137*, 135101.
33. Doye, J. P. K.; Ouldridge, T. E.; Louis, A. A.; Romano, F.; Sulc, P.; Matek, C.; Snodin, B. E. K.; Rovigatti, L.; Schreck, J. S.; Harrison, R. M.; *et al.* Coarse-Graining DNA for Simulations of DNA Nanotechnology. *Phys. Chem. Chem. Phys.* **2013**, *15*, 20395–20414.
34. Saika-Voivod, I.; Smallenburg, F.; Sciortino, F. Understanding Tetrahedral Liquids through Patchy Colloids. *J. Chem. Phys.* **2013**, *139*, 234901.
35. Maldovan, M.; Thomas, E. Diamond Structured Photonic Crystals. *Nat. Mater.* **2004**, *3*, 593–600.
36. Wegener, M. Metamaterials Beyond Optics. *Science* **2013**, *342*, 939–940.
37. Vega, C.; Monson, P. A. Solid-Fluid Equilibrium for a Molecular Model with Short Ranged Directional Forces. *J. Chem. Phys.* **1998**, *109*, 9938–9949.
38. Romano, F.; Sanz, E.; Sciortino, F. Crystallization of Tetrahedral Patchy Particles *in Silico*. *J. Chem. Phys.* **2011**, *134*, 174502.

39. Noya, E. G.; Vega, C.; Doye, J. P. K.; Louis, A. A. Phase Diagram of Model Anisotropic Particles with Octahedral Symmetry. *J. Chem. Phys.* **2007**, *127*, 054501.
40. Doye, J. P. K.; Louis, A. A.; Lin, I.-C.; Allen, L. R.; Noya, E. G.; Wilber, A. W.; Kok, H. C.; Lyus, R. Controlling Crystallization and Its Absence: Proteins, Colloids and Patchy Models. *Phys. Chem. Chem. Phys.* **2007**, *9*, 2197–2205.
41. Doppelbauer, G.; Noya, E. G.; Bianchi, E.; Kahl, G. Self-Assembly Scenarios of Patchy Colloidal Particles. *Soft Matter* **2012**, *8*, 7768–7772.
42. Vega, C.; Sanz, E.; Abascal, J. L. F.; Noya, E. G. Determination of Phase Diagrams *via* Computer Simulation: Methodology and Applications to Water, Electrolytes and Proteins. *J. Phys.: Condens. Matter* **2008**, *20*, 153101–153139.
43. Smith, B.; Frenkel, D. *Understanding Molecular Simulations*; Academic Press: New York, 1996.
44. Romano, F.; Hudson, A.; Doye, J. P. K.; Ouldridge, T. E.; Louis, A. A. The Effect of Topology on the Structure and Free Energy Landscape of DNA Kissing Complexes. *J. Chem. Phys.* **2012**, *136*, 215102.
45. Romano, F.; Chakraborty, D.; Doye, J. P. K.; Ouldridge, T. E.; Louis, A. A. Coarse-Grained Simulations of DNA Overstretching. *J. Chem. Phys.* **2013**, *138*, 085101.
46. Matek, C.; Ouldridge, T. E.; Levy, A.; Doye, J. P. K.; Louis, A. A. DNA Cruciform Arms Nucleate through a Correlated but Asynchronous Cooperative Mechanism. *J. Phys. Chem. B* **2012**, *116*, 11616–11625.
47. De Michele, C.; Rovigatti, L.; Bellini, T.; Sciortino, F. Self-Assembly of Short DNA Duplexes: From a Coarse-Grained Model to Experiments through a Theoretical Link. *Soft Matter* **2012**, *8*, 8388.
48. Kern, N.; Frenkel, D. Fluid-Fluid Coexistence in Colloidal Systems with Short-Ranged Strongly Directional Attraction. *J. Chem. Phys.* **2003**, *118*, 9882–9889.
49. http://dna.physics.ox.ac.uk.
50. Frenkel, D.; Ladd, A. J. C. New Monte Carlo Method To Compute the Free Energy of Arbitrary Solids. Application to the FCC and HCP Phases of Hard Spheres. *J. Chem. Phys.* **1984**, *81*, 3188–3193.